

Title	Influence of pulse duration on mechanical properties and dislocation density of dry laser peened aluminum alloy using ultrashort pulsed laser-driven shock wave
Author(s)	Yoshida, Masayuki; Nishibata, Itsuki; Matsuda, Tomoki et al.
Citation	Journal of Applied Physics. 2022, 132(7), p. 075101
Version Type	VoR
URL	https://hdl.handle.net/11094/89440
rights	This article may be downloaded for personal use only. Any other use requires prior permission of the author and AIP Publishing. This article appeared in Yoshida M., Nishibata I., Matsuda T., et al. Influence of pulse duration on mechanical properties and dislocation density of dry laser peened aluminum alloy using ultrashort pulsed laser-driven shock wave. Journal of Applied Physics, 132(7), 075101 and may be found at https://doi.org/10.1063/5.0083511 .
Note	

The University of Osaka Institutional Knowledge Archive : OUKA

<https://ir.library.osaka-u.ac.jp/>

The University of Osaka

Influence of pulse duration on mechanical properties and dislocation density of dry laser peened aluminum alloy using ultrashort pulsed laser-driven shock wave

Cite as: J. Appl. Phys. **132**, 075101 (2022); <https://doi.org/10.1063/5.0083511>

Submitted: 27 December 2021 • Accepted: 11 July 2022 • Published Online: 16 August 2022

Masayuki Yoshida (吉田 雅幸),  Itsuki Nishibata (西端 樹),  Tomoki Matsuda (松田 朋己), et al.

COLLECTIONS

Paper published as part of the special topic on [Shock Behavior of Materials](#)



View Online



Export Citation



CrossMark

ARTICLES YOU MAY BE INTERESTED IN

[Effect of UV light illumination in humid air on the optical and electronic properties of the orthorhombic \$\alpha\$ -MoO₃ and monoclinic \$\beta\$ -MoO₃](#)

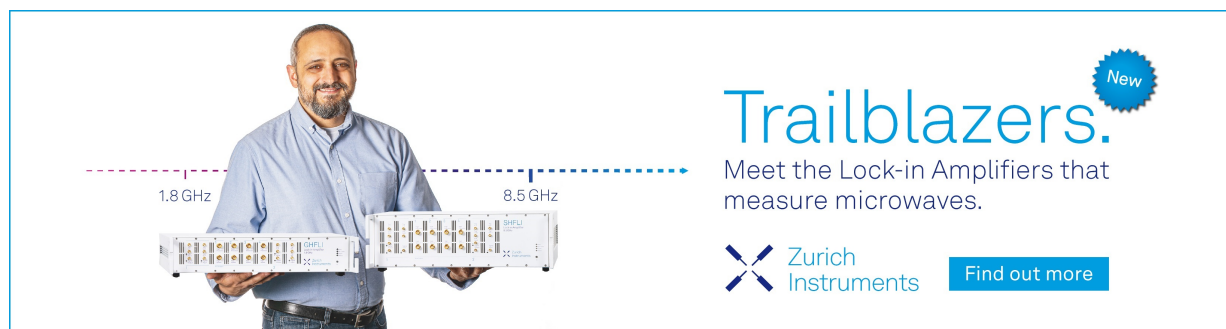
Journal of Applied Physics **132**, 075102 (2022); <https://doi.org/10.1063/5.0095295>


[Experimental and theoretical examination of shock-compressed copper through the fcc to bcc to melt phase transitions](#)

Journal of Applied Physics **132**, 075902 (2022); <https://doi.org/10.1063/5.0088607>


[Surface plasmon resonance enhanced self-powered graphene/Al₂O₃/InGaAs near-infrared photodetector](#)

Journal of Applied Physics **132**, 073102 (2022); <https://doi.org/10.1063/5.0103803>



Trailblazers. 

Meet the Lock-in Amplifiers that measure microwaves.

 Zurich Instruments [Find out more](#)

Influence of pulse duration on mechanical properties and dislocation density of dry laser peened aluminum alloy using ultrashort pulsed laser-driven shock wave

Cite as: J. Appl. Phys. **132**, 075101 (2022); doi: [10.1063/5.0083511](https://doi.org/10.1063/5.0083511)

Submitted: 27 December 2021 · Accepted: 11 July 2022 ·

Published Online: 16 August 2022



View Online



Export Citation



CrossMark

Masayuki Yoshida (吉田 雅幸),¹ Itsuki Nishibata (西端 樹),¹ Tomoki Matsuda (松田 朋己),¹ Yusuke Ito (伊藤 佑介),² Naohiko Sugita (杉田 直彦),² Ayumi Shiro (城 鮎美),³ Takahisa Shobu (菖蒲 敬久),⁴ Kazuto Arakawa (荒河 一渡),⁵ Akio Hirose (廣瀬 明夫),¹ and Tomokazu Sano (佐野 智一)^{1,a)}

AFFILIATIONS

¹Division of Materials and Manufacturing Science, Graduate School of Engineering, Osaka University, Suita, Osaka 565-0871, Japan

²Department of Mechanical Engineering, School of Engineering, The University of Tokyo, Bunkyo, Tokyo 113-8656, Japan

³Quantum Beam Science Research Directorate, National Institute for Quantum and Radiological Science and Technology, Sayo, Hyogo 679-5148, Japan

⁴Materials Sciences Research Center, Japan Atomic Energy Agency, Sayo, Hyogo 679-5148, Japan

⁵Next Generation TATARA Co-Creation Centre, Organization for Industrial Innovation, Shimane University, Matsue, Shimane 690-8504, Japan

Note: This paper is part of the Special Topic on Shock Behavior of Materials.

a) Author to whom correspondence should be addressed: sano@mapse.eng.osaka-u.ac.jp; +81-6-6879-7534; 2-1 Yamada-oka, Suita, Osaka 565-0871, Japan

ABSTRACT

This study aims to investigate the influence of the pulse duration on the mechanical properties and dislocation density of an aluminum alloy treated using dry laser peening (DLP), which is a laser peening technique that uses ultrashort pulsed laser-driven shock wave to eliminate the need for a sacrificial overlay under atmospheric conditions. The results of the micro-Vickers hardness test, residual stress measurement, and dislocation density measurement demonstrate that over a pulse duration range of 180 fs to 10 ps, the maximum peening effects are achieved with a pulse duration of 1 ps. Moreover, the most significant DLP effects are obtained by choosing a pulse duration that achieves a laser intensity that simultaneously generates the strongest shock pressure, suppresses optical nonlinear effects, and realizes the least thermal effects, which weaken the shock effects. Shock temperature calculations based on thermodynamic equations also suggest that a laser intensity driving a shock pressure less than 80 GPa, as in the case of a pulse duration of 1 ps in this study, maintains the solid state of the material throughout the process, resulting in significant DLP effects.

Published under an exclusive license by AIP Publishing. <https://doi.org/10.1063/5.0083511>

I. INTRODUCTION

Peening techniques, such as shot peening,¹ ultrasonic peening,² cavitation peening³ and laser peening,^{4,5} are surface treatment methods aimed at improving mechanical properties, such as fatigue performance and corrosion resistance, by hardening the material and introducing compressive residual stresses on the surface caused by plastic deformation of the material. Laser peening

techniques with a nanosecond pulse laser are currently used in various industries,^{6,7} such as nuclear and aerospace industries. When a material is irradiated with a nanosecond pulse laser, ablation plasma is generated from the material surface. A transparent overlay such as water confines the expansion of the ablation plasma, resulting in a pressure propagation into the material that is sufficiently strong to cause plastic deformation.^{8,9} However, nanosecond laser

TABLE I. Chemical compositions (wt.%) of the 2024-T351 aluminum alloy.

Si	Fe	Cu	Mn	Mg	Cr	Zn	Ti	Al
0.0780	0.0970	4.5790	0.5340	1.5130	0.0010	0.0330	0.0237	Bal.

pulse irradiation causes the melting of the laser irradiated area, resulting in a change of the surface roughness and induction of the tensile residual stress caused by the solidification shrinkage. To prevent the melting, a protective coating, such as a metal film or paint, is applied to the material surface.¹⁰

Meanwhile, dry laser peening (DLP) uses femtosecond laser pulses,^{11–13} which eliminates the need for any plasma confinement medium or protective coating in the air. At a high intensity of femtosecond laser irradiation, thin layers of the surface are removed explosively with more intense laser ablation as compared with that of nanosecond laser irradiation. The recoil pressure of the laser ablation then drives a shock wave propagating into the material.^{14–17} This shock wave reaches more than 100 GPa,¹⁴ which causes the plastic deformation of the material even in air without a plasma confinement medium.^{18,19} Moreover, the thermal effects of femtosecond laser irradiation are smaller than those of nanosecond laser irradiation.²⁰ Thus, DLP using a femtosecond laser suppresses the change of the surface roughness and induces a compressive residual stress without a protective coating and plasma confinement medium in air.

When the laser intensity exceeds 1013 W/cm² in the air, optical nonlinear phenomena, e.g., air breakdown and optical Kerr effect, occur. Such phenomena cause defocusing, turbulence of the spatial energy distribution, and energy loss, resulting in the difference between the laser ablation phenomena in vacuum and air.^{21–25} These optical nonlinear phenomena in air are suggested to influence DLP effects. Moreover, the pulse duration, which is one of the laser-irradiation conditions, is considered to have a significant effect on the shock-affected zone and heat-affected zone introduced by the DLP. It was reported that the most compressive residual stress is induced with a pulse duration of 1.0 ps ranging from 180 fs to 10 ps using the wavelength of 1028 nm with the $1/e^2$ diameter of 3.5 mm, indicating the existence of optimum pulse durations for DLP.²⁶ However, the influence of the pulse duration on the amount of plastic deformation, which is the direct source of peening effects, has never been reported.

This study aims to investigate the influence of the pulse duration ranging from femtoseconds to picoseconds on the ablation properties, mechanical properties such as hardness and residual stress, and dislocation density of DLPed specimens. To evaluate the influence of the pulse duration on the intensity of the laser ablation, which is the driving force of the shock wave, the crater depth formed by the laser ablation is measured. Furthermore, hardness and residual stress values were measured to evaluate the effects of the pulse duration on laser peening. The dislocation density, which reflects the extent of plastic deformation caused by the ultrashort pulsed laser-driven shock wave that influence the peening effects, is also evaluated through microstructure observations and diffraction profiles using transmission electron microscopy (TEM) and x-ray diffraction (XRD), respectively.

The temperature in a shock-compressed solid rises due to entropy enhancement.²⁷ The shocked-solid melts above a threshold

pressure due to the rise in its own temperature. When an ultrashort laser pulse is irradiated on the material, the heat affected zone due to laser heating is negligibly small. However, the influence of the rise in temperature due to the ultrashort laser-driven shock compression on the material has never been investigated. Herein, we also investigate the relationships between the temperature rise and the DLP effects.

II. METHODS

A. Specimens

In this study, the 2024-T351 aluminum alloy with a thickness of 10 mm was used as a specimen. The T351 treatment relieved the residual stress by stretching after solution heat treatment. The chemical composition and mechanical properties of the specimens are listed in [Tables I and II](#), respectively.

B. Dry laser peening

Schematic illustrations of the DLP experiment are shown in [Fig. 1](#). Ultrashort laser pulses with a wavelength of 1028 nm and pulse energy of 0.95 mJ (PHAROS, Light Conversion) were focused using a plano-convex lens with a focal length of 70 mm onto the specimen in air, as shown in [Fig. 1\(a\)](#). The specimen was mounted on an X-Y automatic stage, and the specimen was moved in the X and Y directions during the laser irradiation as shown in [Fig. 1\(b\)](#). The laser pulses were overlapped with a coverage C_v of 700%. Here, the coverage is expressed as $C_v = A_p N_p \times 100$ (%), where A_p is the crater area, and N_p is the number of pulses per unit area. Pulse durations of 180 fs, 500 fs, 1 ps, 5 ps, and 10 ps were selected for the DLP conditions based on the results of the relationship between the ablation depth and pulse duration.

C. Ablation properties

The irradiated area was observed using scanning electron microscopy (SEM, JSM-IT500, JEOL), and the depth of the crater formed by eight pulses was measured using a confocal laser scanning microscope (VK-9700, Keyence Corporation). The ablation depth per pulse was estimated by dividing the crater depth by the number of pulses.

TABLE II. Mechanical properties of the 2024-T351 aluminum alloy.

0.2% proof stress (MPa)	Tensile strength (MPa)	Elongation (%)
321	464	19.2

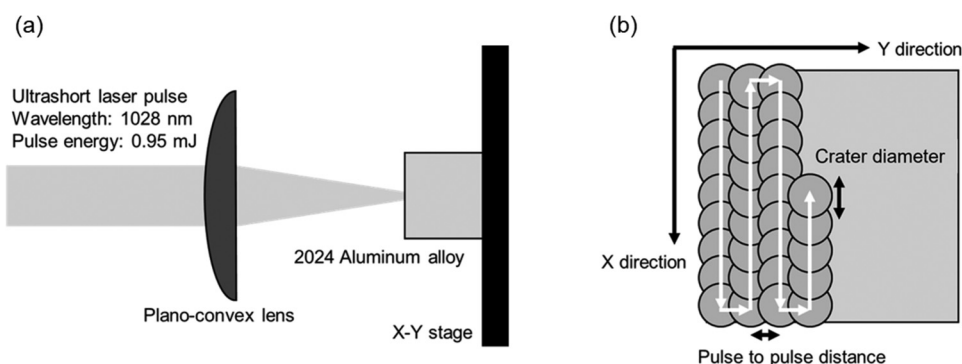


FIG. 1. Schematic illustrations of the experimental setup of dry laser peening. (a) Irradiation method of ultrashort pulse laser and (b) scan direction of the ultrashort laser pulses.

D. Surface roughness

The surface roughness of the unirradiated and DLPed specimens was measured using a confocal laser scanning microscope. The arithmetic mean roughness (R_a) was used for the surface roughness value. The surface of the DLPed specimens was observed using SEM.

E. Hardness

The surface hardness of the unirradiated and DLPed specimens was measured using the micro-Vickers hardness test. It was performed with a load of 0.98 N and a dwell time of 15 s. Before the hardness test, the debris layer formed on surface of the DLPed specimens were removed by the electropolishing because the debris layer does not contribute to the DLP effects. The thickness of debris layer is about a few micrometers.

F. Residual stress

The residual stress on the surface of the DLPed specimens was measured using the $\cos\alpha$ method²⁸ (μ -X360s, Pulstec Industrial Co., Ltd.) using a $\text{CrK}\alpha$ x ray with a wavelength of 0.2291 nm, where the 311 reflection of Al was used with a Young's modulus of $E = 69.31$ GPa and a Poisson's ratio of $\nu = 0.348$. Thin layers of the surface were successively removed by electrolytic polishing to obtain the depth profile of the residual stress. A 10% HClO_4 solution was used for polishing at an applied voltage of 16 V under a constant temperature of 0 °C. The residual stress introduced by DLP is larger in the Y direction than in the X direction. In this experiment, the residual stress in the Y direction was measured to clarify the difference due to the pulse durations.

G. Dislocation density

The dislocation density in the DLPed specimens was estimated using TEM (Talos F200i, Thermo Fisher Scientific K.K.) with an accelerating voltage of 200 kV. For the TEM observations, a thin cross-section specimen was cut from the surface layer in the specimens using a focused Ga^+ ion beam (Scios 2 DualBeam System, Thermo Fisher Scientific K.K.). The thickness of the piece was approximately 100 nm. Moreover, the specimen surfaces were covered with platinum before cutting to prevent damage caused by

the ion beam. The dislocation density was quantitatively estimated using the Keh's method (see Ref. 12).

The dislocation density was also estimated through a nondestructive XRD measurements using the Williamson-Hall equation as expressed by $\Delta K = 0.9/D + \langle \epsilon \rangle K$,²⁹ where D is the crystallite size, $\langle \epsilon \rangle$ is the plastic strain, K is the length of the diffraction vector given by $K = 2 \sin \theta / \lambda$, and $\Delta K = 2 \cos \theta (\Delta 2\theta) / \lambda$, where θ and λ are the diffraction angle and wavelength of the x rays, respectively. The dislocation density ρ is expressed as $\rho = 2\sqrt{3} \langle \epsilon \rangle / Db$, where b is the magnitude of the Burgers vector. The XRD measurements were performed using x rays with a photon energy of 30.024 keV at the BL22XU beamline of SPring-8, as shown in Fig. 2.³⁰ The diffracted x rays were detected using a CdTe detector. The size of the incident and receiving slits were 200 μm in the horizontal direction and 5 μm in the vertical direction. The diffraction angle and full width at half maximum (FWHM) of the normalized line profiles of reflections in the gauge volume were measured to evaluate strain states and estimate the dislocation density.

III. RESULTS

A. Ablation properties

Figure 3 shows the SEM images of the irradiated area with pulse durations of 180 fs, 1 ps, and 10 ps. As shown in Fig. 3(a), the

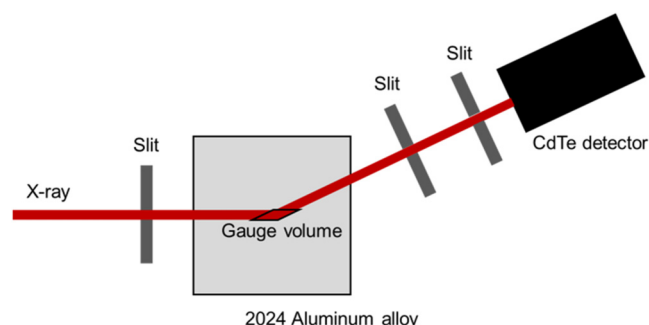


FIG. 2. Schematic illustrations of the experimental setup of the strain scanning method.

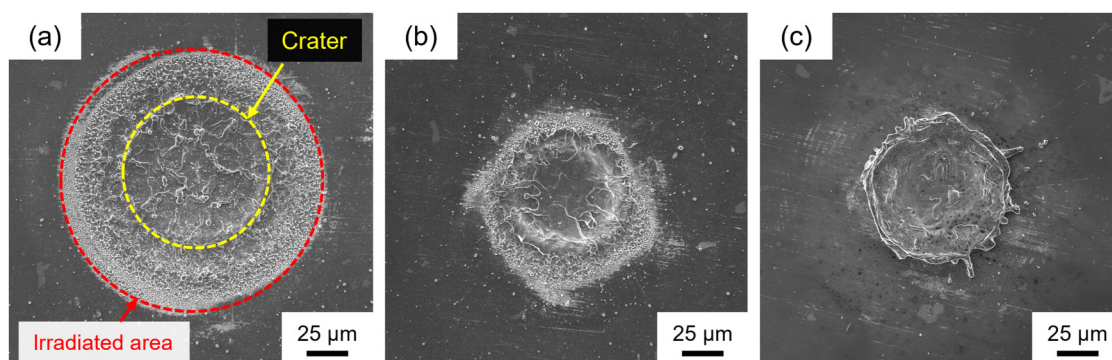


FIG. 3. SEM images of the irradiation area at the focal position of the laser pulses with pulse duration of (a) 180 fs, (b) 1 ps, and (c) 10 ps. The region surrounded by the red dotted line indicates the irradiated area, where the metal surface is discolored by laser ablation. The region surrounded by the yellow dotted line indicates the crater, where the metal surface is intensely etched by laser ablation in the center of the irradiated area.

region in which the metal surface is discolored by laser ablation is defined as the irradiated area, and the region intensely etched by laser ablation in the center of the irradiated area is defined as the crater. Table III shows the irradiated area diameter and crater diameter for each laser irradiation condition. In this experiment, the fluence and intensity are calculated by defining the irradiated area diameter as the beam diameter. The irradiated areas with a pulse duration of 180 and 500 fs are larger than those under other conditions at the focus position, resulting in decreased fluence. The result suggests that the effects of optical nonlinear phenomena increase as the pulse duration decreases. Moreover, Fig. 3(c) shows numerous melt droplets in the irradiated area using a pulse duration of 10 ps. Since the fluence for pulse durations of 1 and 10 ps is the same, the result suggests that the thermal effects increase as the pulse duration increases.

The relationship between the ablation depth per pulse and the pulse duration is shown in Fig. 4. The ablation depths of 12 craters were measured, and the average values, excluding the maximum and minimum values, were plotted. The error bars show the maximum and minimum values of the ablation depths of the irradiation craters. The maximum ablation depth is $0.89 \mu\text{m}/\text{pulse}$ at a pulse duration of 700 fs. When the pulse duration was lower than 700 fs, the ablation depth decreased with a decrease in the pulse duration. Meanwhile, with a longer pulse duration, the ablation depth decreased with an increase in the pulse duration.

TABLE III. Irradiation area diameter and crater diameter at focal position in each laser irradiation condition.

Pulse duration	Irradiation area diameter (μm)	Crater diameter (μm)	Fluence (J/cm^2)	Intensity (W/cm^2)
180 fs	140	70	6	3.4×10^{13}
500 fs	110	60	10	2.0×10^{13}
1 ps	80	60	19	1.9×10^{13}
5 ps	80	60	19	3.8×10^{12}
10 ps	80	60	19	1.9×10^{12}

B. Surface roughness

The results of the surface roughness measurement for the unirradiated and DLPed specimens are shown in Fig. 5. The surface roughness was measured at four points for each specimen and the average values are indicated. The error bars show the maximum and minimum values of the surface roughness. The surface roughness of the unirradiated specimen was $0.05 \mu\text{m}$ while that of the DLPed specimens increased. The maximum surface roughness is $1.57 \mu\text{m}$ at a pulse duration of 1 ps. These results are in good agreement with the relationship between pulse durations and the ablation depth. Figure 6 shows the SEM images of the DLPed specimen surface with pulse durations of 180 fs, 1 ps, and 10 ps. A debris layer was formed by the laser ablation on the surface of DLPed specimens. These results suggest that the most intense laser ablation occurred at a pulse duration of 1 ps.

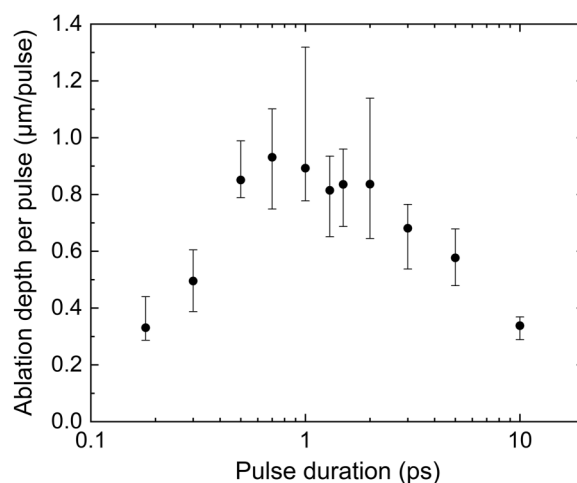


FIG. 4. Relationship between the ablation depth per pulse and pulse duration.

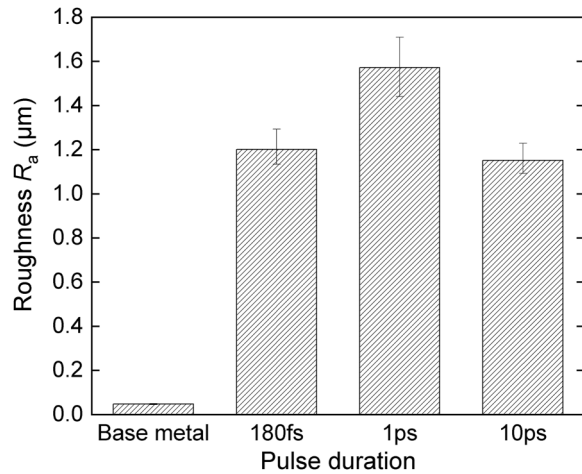


FIG. 5. Surface roughness values of the unirradiated and DLPed specimen.

C. Hardness

The results of the micro-Vickers hardness test for the unirradiated and DLPed specimens are shown in Fig. 7. The surface hardness test was performed at 12 points for each specimen. The average values, excluding the maximum and minimum values, are indicated. The error bars show the maximum and minimum values of the surface hardness. The surface hardness of the unirradiated specimen was 146 HV while the hardness of the DLPed specimens increased. This is attributed to the work hardening caused by plastic deformation. The maximal surface hardness was 202 HV at a pulse duration of 1 ps. Above 1 ps, the surface hardness decreased with the increasing pulse duration. Below 1 ps, as the pulse duration decreased, the surface hardness also decreased.

D. Residual stress

The depth profiles of the residual stress in the DLPed specimens are shown in Fig. 8. The error bars show the standard deviation value. The pulse duration of 1 ps introduced the maximum compressive residual stress of approximately 400 MPa at

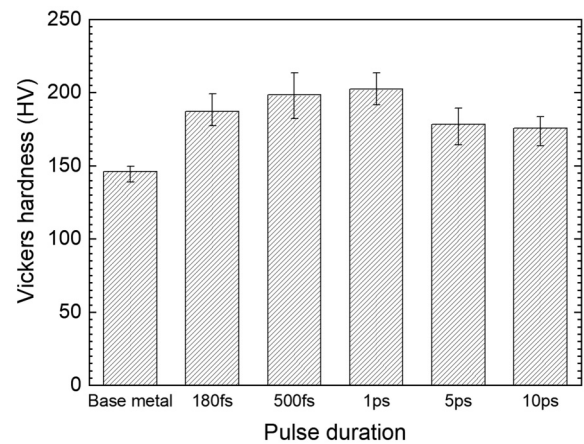


FIG. 7. Hardness values of the surfaces of the unirradiated and DLPed specimen.

a depth of $4\mu\text{m}$ from the surface. This value is almost equal to the 0.2% proof stress of the 2024-T351 aluminum alloy. Above 1 ps, the maximum compressive stress value and the depth at which the compressive residual stress is introduced decreased as the pulse duration increased. Below 1 ps, as the pulse duration decreased, the maximum compressive stress value decreased, but the depth at which compressive residual stress is formed remained the same.

E. Dislocation density

Figure 9 shows the TEM images of the cross sections of the unirradiated and DLPed specimen with pulse durations of 180 fs, 1 ps, and 10 ps. The regions observed using TEM is the solid phase area with the highest dislocation density in the each DLPed specimen. To clearly observe dislocations as black lines, the incident direction of the electron beam is displaced from crystal zone axes and the excite 111 reflections of aluminum. We find high-density dislocations are formed in the specimen. The dislocation densities estimated in the unirradiated and DLPed specimens (Fig. 9) are listed in Table IV. The error bars show uncertainty in the thickness of TEM observation specimen. The dislocation density in the

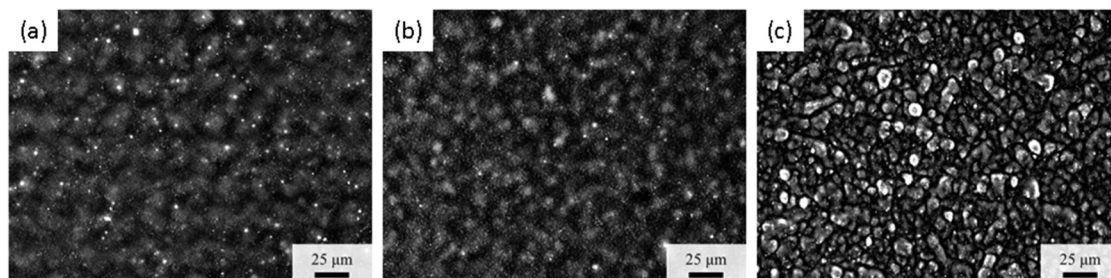


FIG. 6. SEM images of the DLPed specimen surfaces with pulse duration of (a) 180 fs, (b) 1 ps, and (c) 10 ps.

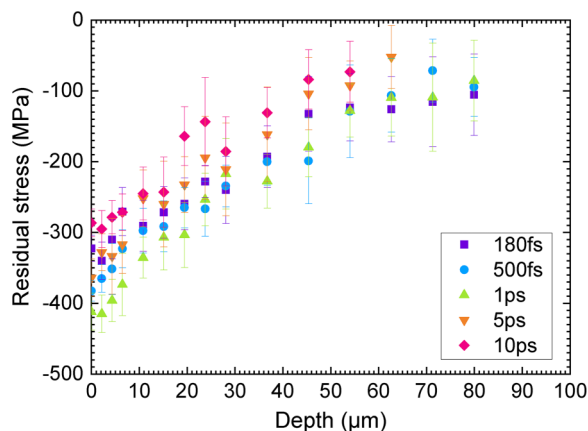


FIG. 8. Residual stress distribution in the DLPed specimen.

TABLE IV. Dislocation density in the DLPed specimen estimated using the Keh equation.

Pulse duration	Dislocation density (m^{-2})
Base metal	2.3×10^{14}
180 fs	6.7×10^{14}
1 ps	8.3×10^{14}
10 ps	5.5×10^{14}

unirradiated sample was $2.3 \times 10^{14} \text{ m}^{-2}$. Meanwhile, the values increased in the DLPed specimen with pulse durations of 180 fs, 1 ps, and 10 ps. A sufficient impact force to induce plastic deformation was applied to the specimen even under a pulse duration of 10 ps. The maximum dislocation density is $8.3 \times 10^{14} \text{ m}^{-2}$ under a pulse duration of 1 ps. Therefore, the strongest shock wave occurred with a pulse duration of 1 ps.

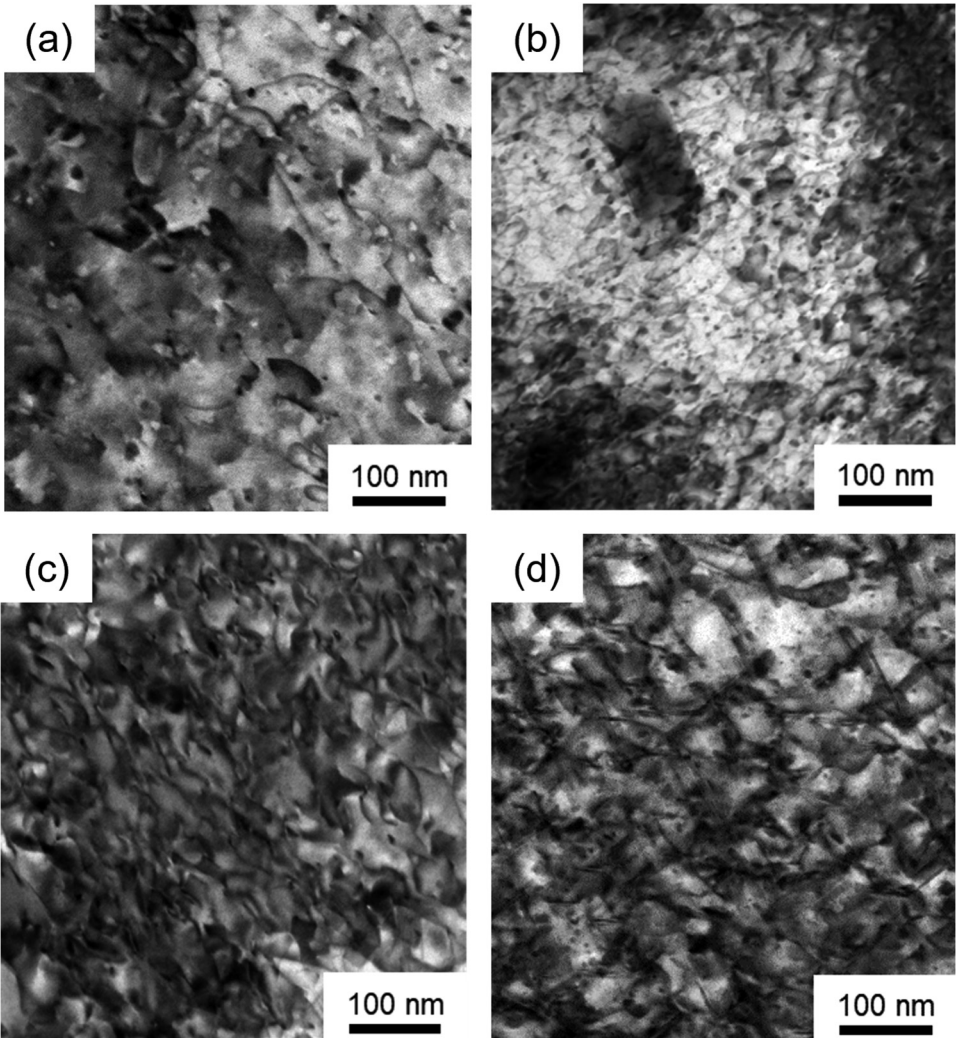


FIG. 9. TEM images of the solid phase region in (a) the base metal, and in the DLPed specimen with a pulse duration of (b) 180 fs, (c) 1 ps, and (d) 10 ps.

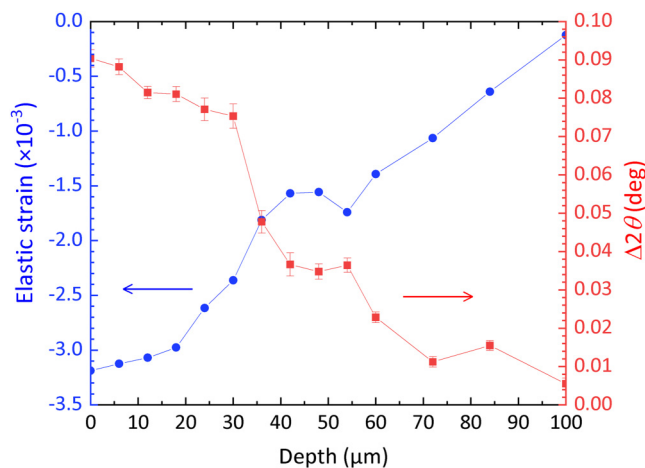


FIG. 10. Residual elastic strain and $\Delta 2\theta$ distributions in the Y direction in the DLPed specimen with a pulse duration of 1 ps.

Figure 10 shows the depth profile of the residual elastic strain and $\Delta 2\theta$ in the DLPed specimen with a pulse duration of 1 ps measured by XRD. The error bars for $\Delta 2\theta$ show the standard deviation, whereas the error bars for the elastic strain are included in the plots. The compressive elastic and plastic strains in the Y-direction exist from the surface to a depth of approximately $100\text{ }\mu\text{m}$ and increase as the depth becomes shallower.

The dislocation density in the DLPed specimen with a pulse duration of 1 ps was quantitatively estimated using the Williamson-Hall equation. The dislocation densities at a depth of $8\text{ }\mu\text{m}$ with a large amount of plastic strain introduced as shown in Fig. 10 were estimated in this experiment. Table V shows the plastic strain, crystallite size, and dislocation density. The region appeared to be plastically deformed by an ultrashort pulsed laser-driven shock wave and formed dislocations with a density of $9.4 \times 10^{14}\text{ m}^{-2}$ in the X direction and $7.7 \times 10^{14}\text{ m}^{-2}$ in the Y direction. These results agree well with the dislocation densities estimated from TEM observations. Laser irradiation with a pulse duration of 1 ps drives a sufficiently strong impact force to introduce plastic deformation in air.

IV. DISCUSSION

A. Effects of optical nonlinear phenomena

Mechanical properties, such as the hardness, residual stress, and dislocation density, of the DLPed 2024 aluminum alloy as well as the ablation depth per pulse are dependent on the pulse

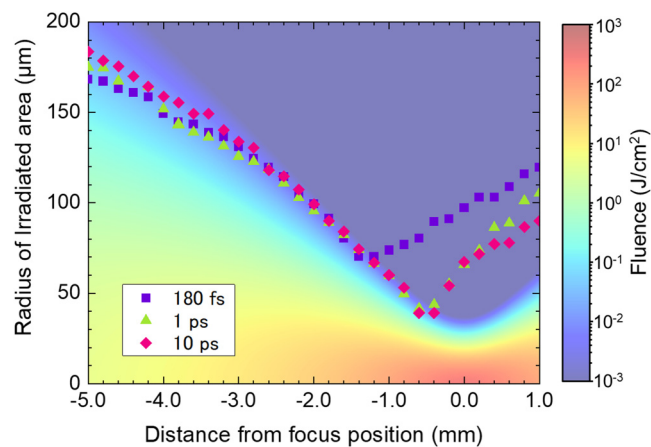


FIG. 11. Irradiated area radius over the fluence distribution map, which assumes Gaussian beam focusing propagation, as a function of the distance from the focal position.

duration, with 1 ps as the optimal duration. Here, we discuss the influence of the pulse duration on the ablation depth, which reflects both the shock and thermal effects induced by laser irradiation. Above 1 ps, as the pulse duration increased, the crater depth decreased and the melted region widened around the irradiated area, which suggested that thermal effects, such as heat diffusion, dominated over the shock effects.³⁰ Below 1 ps, as the pulse duration decreased, the crater depth decreased and the irradiated area increased, which suggested a decrease in the laser fluence. Droffog *et al.* and Nielsen *et al.* reported that for an ultrashort pulsed laser with a pulse duration below 1 ps, the amount of ablation was less dependent on the pulse durations.^{31,32} However, this was not observed in our study. For the DLP using an ultrashort pulsed laser with a laser intensity ranging from 10^{14} to 10^{16} W/cm^2 , the interaction of the laser pulse with air must be considered. Figure 11 shows the radius of the irradiated area measured from the SEM images plotted over the fluence distribution, which assumes a Gaussian beam focusing under ideal light propagation, as a function of the distance from the focus position. Here, the negative direction indicates the laser incident side. As shown in Fig. 11, the irradiation area with a pulse duration of 180 fs was larger than those with a pulse duration of 1 and 10 ps. Moreover, the focal point of the beam shifted to the laser-incident side at a pulse duration of 180 fs. These are caused by nonlinear optical phenomena, e.g. the optical Kerr effect and air breakdown. The high laser intensities associated with short pulse durations amplify the nonlinear optical effects, resulting in an increase in the irradiation area and a decrease in

TABLE V. Microstructure characteristics in the specimen after DLP, irradiated with a pulse duration of 1 ps.

Direction	Plastic strain ($\times 10^{-3}$)	Crystallite size (nm)	Dislocation density ($\times 10^{14}\text{ m}^{-2}$)
X direction	7.7 ± 0.75	Average: 99 Min.: 59 Max.: 295	Average: 9.4 Min.: 3.4 Max.: 12.9
Y direction	5.9 ± 0.97	Average: 93 Min.: 52 Max.: 471	Average: 7.7 Min.: 1.8 Max.: 11.6

the laser fluence. This eventually lowers the shock effects. Thus, the most significant DLP effects are achieved by choosing a pulse duration that achieves a laser intensity that simultaneously generates the strongest shock pressure, suppresses optical nonlinear effects, and realizes the least thermal effects, which weaken the material plasticity.

B. Temperature under shocked state

The thermodynamic equation under a steady shocked state derived by Walsh and Christian is expressed as:

$$C_{VH} \frac{dT_H}{dV_H} + \frac{\gamma_0}{V_0} C_{VH} T_H = \frac{1}{2} \frac{dp_H}{dV_H} (V_0 - V_H) + \frac{1}{2} (p_H - p_0), \quad (1)$$

where p is the pressure, V is the specific volume, T is the temperature, C_V is the constant-volume specific heat, γ is the Grüneisen parameter, and subscript 0 and H indicate an ambient and a shocked state, respectively.²⁷ For an overdriven-shocked state with the strain rate of 10^{11} – 10^{12} s^{−1} induced by a shock pressure of 200–300 GPa, the equation of state in the shocked solid is expressed using the thermodynamic equation because such a state is steady enough for times longer than electron-phonon relaxation time of 10–100 fs.^{33–35} Therefore, the temperature in the femtosecond laser-driven shocked state is derived from Eq. (1) because the duration of femtosecond laser-driven shock wave is longer than several picoseconds.¹⁷ Pressure P_R and temperature T_R under pressure release, which is an adiabatic process, are expressed as

$$P_R = P_H + 3Nk_B \frac{\gamma_0}{V_0} (T_R - T_H), \quad (2)$$

$$T_R = T_H \exp \left[\frac{\gamma_0}{V_0} (V_H - V) \right], \quad (3)$$

where N is the number of atoms per unit mass and k_B is Boltzmann constant.

Figure 12 shows temperatures under shocked state and under pressure release calculated using Eqs. (1)–(3). The data used for the calculations are listed in Table I in Ref. 34. The melting curve shown here is Moriarty's data.³⁶ The temperature under shocked state and melting curve intersect at 117 GPa, which agree well with the experimental data as reported in Ref. 37. When the shock pressure is less than 80 GPa, release curves do not intersect the melting curve, which indicates that the state remains solid during both rise and fall in pressure. When the shock pressure is 100 GPa, the release curve intersects the melting curve at 23 GPa, indicating melting of material during pressure release. Namely, the material's states are classified for three parts: (i) a solid state during both rise and fall in pressure below the shock pressure of 80 GPa, (ii) a solid state under pressure rise and liquid state during pressure release above 80 GPa and less than 117 GPa of the shock pressure, and (iii) liquid state during pressure rise above 117 GPa of the shock pressure.

The laser intensities used are 3.4×10^{13} and 1.9×10^{13} W/cm² for pulse durations of 180 fs and 1 ps, respectively. Shock pressures driven by these laser pulses are around 100 and 20 GPa for pulse duration of 180 fs and 1 ps, respectively, which are derived using the relationships

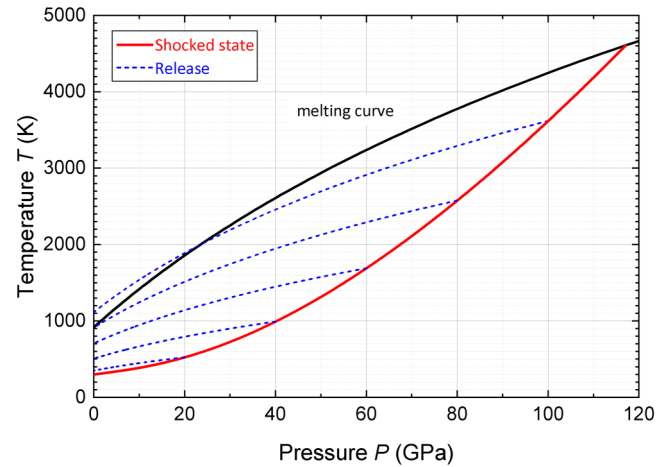


FIG. 12. Temperatures under shocked state and under pressure release calculated using thermodynamic equations.

between femtosecond laser intensity and shock pressure, experimentally obtained by Ionin *et al.*³⁸ Despite that the laser intensity and resulting shock pressure for the pulse duration of 180 fs are larger than those for the pulse duration of 1 ps, the dislocation density which indicates the amount of plastic deformation for the pulse duration of 180 fs is smaller than that for the pulse duration of 1 ps, which suggests dislocation annihilation caused by melting during pressure release for the shock pressure of 100 GPa. The calculations clarify that a laser intensity driving a shock pressure of less than 80 GPa maintains the solid state of the material, leading to significant DLP effects.

V. CONCLUSIONS

The influence of the pulse duration on the peening effects in the DLPed aluminum alloy was investigated. Mechanical properties, such as the hardness, residual stress, and dislocation density, as well as the crater depth per pulse of the alloy was dependent on the pulse duration. The maximal ablation depths were 0.89 to 0.93 $\mu\text{m}/\text{pulse}$ at pulse durations of 700 fs and 1 ps. A surface hardness of 202 HV, a compressive residual stress of approximately 400 MPa, and a dislocation density of $9.4 \times 10^{14} \text{ m}^{-2}$ were the optimal values, obtained at a pulse duration of 1 ps. These results indicate that the strongest shock effect was induced at a pulse duration of 1 ps. As the pulse duration increased above this optimal value, thermal effects, such as heat diffusion, dominated the shock effects. Meanwhile, the laser fluence decreased as the pulse duration decreased below 1 ps owing to the broadening of the irradiated area caused by the effect of nonlinear optical phenomena, e.g., air breakdown and the optical Kerr effect. A pulse duration of 1 ps simultaneously generates the strongest shock pressure, suppresses optical nonlinear effects, and realizes the least thermal effects that weaken the shock effects, resulting in the most effective DLP. Shock temperature calculations based on thermodynamic equations suggest that a laser intensity driving shock pressure of less than 80 GPa remains the solid state of the material, resulting in significant DLP effects.

ACKNOWLEDGMENTS

This study was supported in part by MEXT Quantum Leap Flagship Program (MEXT Q-LEAP) Grant No. JPMXS0118068348, JSPS KAKENHI Grant Nos. 19K22061 and 20H02048, The Amada Foundation, The Light Metal Educational Foundation, Inc., Osawa Scientific Studies Grants Foundation, and Mazak Foundation. The synchrotron radiation experiments were performed at the JAEA beamline BL22XU of SPring-8 under the Shared Use Program of QST (Proposal Nos. 2018B-H12 and 2020A-H23) facilities with the approval of Nanotechnology Platform project supported by the Ministry of Education, Culture, Sports, Science and Technology (Proposal Nos. A-18-QS-0031 and A-20-QS-0022) and the approval of the Japan Synchrotron Radiation Research Institute (JASRI) (Proposal Nos. 2018B3683, 2020A3784, 2021A3723 and 2021B3723).

AUTHOR DECLARATIONS

Conflict of Interest

The authors have no conflicts to disclose.

Author Contributions

Masayuki Yoshida: Conceptualization (equal); Formal analysis (equal); Investigation (equal); Methodology (equal); Visualization (equal); Writing – original draft (equal). **Itsuki Nishibata:** Methodology (equal). **Tomoki Matsuda:** Investigation (equal). **Yusuke Ito:** Methodology (equal); Writing – review and editing (equal). **Naohiko Sugita:** Writing – review and editing (equal). **Naohiko Sugita:** Writing – review and editing (equal). **Naohiko Sugita:** Writing – review and editing (equal). **Naohiko Sugita:** Writing – review and editing (equal). **Ayumi Shiro:** Investigation (equal); Methodology (equal). **Takahisa Shobu:** Investigation (equal); Methodology (equal); Writing – review and editing (equal). **Kazuto Arakawa:** Investigation (equal); Methodology (equal). **Akio Hirose:** Investigation (equal). **Tomokazu Sano:** Conceptualization (equal); Funding acquisition (equal); Investigation (equal); Methodology (equal); Project administration (equal); Resources (equal); Supervision (equal); Validation (equal); Writing – original draft (equal); Writing – review and editing (equal).

DATA AVAILABILITY

The data that support the findings of this study are available from the corresponding author upon reasonable request.

REFERENCES

- ¹L. Wagner, *Shot Peening* (WILEY-VCH Verlag GmbH & Co. KGaA, Weinheim, 2003).
- ²M. Malaki and H. Ding, *Mater. Des.* **87**, 1072 (2015).
- ³H. Soyama and F. Takeo, *J. Mater. Process. Technol.* **227**, 80 (2016).
- ⁴P. Peyre, R. Fabbro, P. Merrien, and H. P. Lieurade, *Mater. Sci. Eng. A* **210**, 102 (1996).
- ⁵A. H. Clauer, *Metals* **9**, 626 (2019).
- ⁶Y. Sano, M. Obata, T. Kubo, N. Mukai, M. Yoda, K. Masaki, and Y. Ochi, *Mater. Sci. Eng. A* **417**, 334 (2006).
- ⁷R. D. Tenaglia and D. F. Lahrman, *Nat. Photonics* **3**, 267 (2009).
- ⁸Y. Sano, K. Masaki, T. Gushi, and T. Sano, *Mater. Des.* **36**, 809 (2012).
- ⁹R. Fabbro, P. Peyre, L. Berthe, and X. Scherpereel, *J. Laser Appl.* **10**, 265 (1998).
- ¹⁰Y. Liao, C. Ye, and G. J. Cheng, *Opt. Laser Technol.* **78**, 15 (2016).
- ¹¹T. Sano, T. Eimura, R. Kashiwabara, T. Matsuda, Y. Isshiki, A. Hirose, S. Tsutsumi, K. Arakawa, T. Hashimoto, K. Masaki, and Y. Sano, *J. Laser Appl.* **29**, 012005 (2017).
- ¹²T. Kawashima, T. Sano, A. Hirose, S. Tsutsumi, K. Masaki, K. Arakawa, and H. Hori, *J. Mater. Process. Technol.* **262**, 111 (2018).
- ¹³T. Sano, T. Eimura, A. Hirose, Y. Kawahito, S. Katayama, K. Arakawa, K. Masaki, A. Shiro, T. Shobu, and Y. Sano, *Metals* **9**, 1192 (2019).
- ¹⁴R. Evans, A. D. Badger, F. Fallières, M. Mahdih, T. A. Hall, P. Audebert, J. P. Geindre, J. C. Gauthier, A. Mysyrowicz, G. Grillon, and A. Antonetti, *Phys. Rev. Lett.* **77**, 3359 (1996).
- ¹⁵J. C. Crowhurst, M. R. Armstrong, K. B. Knight, J. M. Zaug, and E. M. Behymer, *Phys. Rev. Lett.* **107**, 144302 (2011).
- ¹⁶J. P. Cuq-Lelandais, M. Boustie, L. Berthe, T. de Rességuier, P. Combis, J. P. Colombier, M. Nivard, and A. Claverie, *J. Phys. D: Appl. Phys.* **42**, 065402 (2009).
- ¹⁷V. H. Whitley, S. D. McGrane, D. E. Eakins, C. A. Bolme, D. S. Moore, and J. F. Bingert, *J. Appl. Phys.* **109**, 013505 (2011).
- ¹⁸T. Sano, H. Mori, E. Ohmura, and I. Miyamoto, *Appl. Phys. Lett.* **83**, 3498 (2003).
- ¹⁹T. Matsuda, T. Sano, K. Arakawa, and A. Hirose, *Appl. Phys. Lett.* **105**, 083903 (2014).
- ²⁰B. N. Chichkov, C. Momma, S. Nolte, F. von Alvensleben, and A. Tünnermann, *Appl. Phys. A: Mater. Sci. Process.* **63**, 109 (1996).
- ²¹N. N. Nedialkov, S. E. Imamova, and P. A. Atanasov, *J. Phys. D: Appl. Phys.* **37**, 638 (2004).
- ²²W. Hu, Y. C. Shin, and G. King, *Appl. Phys. Lett.* **99**, 234104 (2011).
- ²³C. Pasquier, M. Sentis, O. Utéza, and N. Sanner, *Appl. Phys. Lett.* **109**, 051102 (2016).
- ²⁴S. S. Mao, X. Mao, R. Greif, and R. E. Russo, *Appl. Phys. Lett.* **77**, 2464 (2000).
- ²⁵X. Zhao and Y. C. Shin, *Appl. Surf. Sci.* **283**, 94 (2013).
- ²⁶I. Nishibata, M. Yoshida, Y. Ito, N. Sugita, A. Hirose, and T. Sano, *Appl. Phys. Express* **14**, 062001 (2021).
- ²⁷J. M. Walsh and R. H. Christian, *Phys. Rev.* **97**, 1544 (1955).
- ²⁸K. Tanaka, *Mech. Eng. Rev.* **6**, 18-00378 (2019).
- ²⁹G. K. Williamson and W. H. Hall, *Acta Metall.* **1**, 22 (1953).
- ³⁰T. Shobu, J. Mizuki, K. Suzuki, Y. Akiniwa, and K. Tanaka, *JSME Int. Journal, Ser. A Solid Mech. Mater. Eng.* **49**, 376 (2006).
- ³¹J. Byskov-Nielsen, J. M. Savolainen, M. S. Christensen, and P. Balling, *Appl. Phys. A: Mater. Sci. Process.* **103**, 447 (2011).
- ³²B. Le Drogoff, F. Vidal, S. Laville, M. Chaker, T. Johnston, O. Barthélemy, J. Margot, and M. Sabsabi, *Appl. Opt.* **44**, 278 (2005).
- ³³Y. Sano and A. Abe, *J. Appl. Phys.* **89**, 105 (2001).
- ³⁴T. Sano and Y. Sano, *J. Appl. Phys.* **90**, 3754 (2001).
- ³⁵T. Sano and Y. Sano, *J. Appl. Phys.* **90**, 5576 (2001).
- ³⁶J. A. Moriarty, D. A. Young, and M. Ross, *Phys. Rev. B* **30**, 578 (1984).
- ³⁷R. G. McQueen, J. N. Fritz, and C. E. Morris, in *Shock Waves in Condensed Matter-1983*, edited by J. R. Asay, R. A. Graham, and G. K. Straub (Elsevier, North-Holland, Amsterdam, 1984), p. 94.
- ³⁸A. A. Ionin, S. I. Kudryashov, S. V. Makarov, L. V. Seleznev, and D. V. Sinitsyn, *JETP Lett.* **94**, 34 (2011).